



## Determination of the temperature coefficient of resistance from micro four-point probe measurements

Marangoni, Thomas ; Guralnik, Benny; Borup, Kasper A.; Hansen, Ole; Petersen, Dirch Hjorth

*Published in:*  
Journal of Applied Physics

*Link to article, DOI:*  
[10.1063/5.0046591](https://doi.org/10.1063/5.0046591)

*Publication date:*  
2021

*Document Version*  
Publisher's PDF, also known as Version of record

[Link back to DTU Orbit](#)

*Citation (APA):*  
Marangoni, T., Guralnik, B., Borup, K. A., Hansen, O., & Petersen, D. H. (2021). Determination of the temperature coefficient of resistance from micro four-point probe measurements. *Journal of Applied Physics*, 129, Article 165105. <https://doi.org/10.1063/5.0046591>

---

### General rights

Copyright and moral rights for the publications made accessible in the public portal are retained by the authors and/or other copyright owners and it is a condition of accessing publications that users recognise and abide by the legal requirements associated with these rights.

- Users may download and print one copy of any publication from the public portal for the purpose of private study or research.
- You may not further distribute the material or use it for any profit-making activity or commercial gain
- You may freely distribute the URL identifying the publication in the public portal

If you believe that this document breaches copyright please contact us providing details, and we will remove access to the work immediately and investigate your claim.


# Determination of the temperature coefficient of resistance from micro four-point probe measurements

Cite as: J. Appl. Phys. **129**, 165105 (2021); <https://doi.org/10.1063/5.0046591>

Submitted: 04 February 2021 . Accepted: 08 April 2021 . Published Online: 27 April 2021

 Thomas A. Marangoni,  Benny Guralnik,  Kasper A. Borup,  Ole Hansen, and  Dirch H. Petersen

## COLLECTIONS

 This paper was selected as Featured



View Online



Export Citation



CrossMark

## ARTICLES YOU MAY BE INTERESTED IN

[Effects of flexoelectricity and strain gradient on bending vibration characteristics of piezoelectric semiconductor nanowires](#)

Journal of Applied Physics **129**, 164301 (2021); <https://doi.org/10.1063/5.0038782>

[Progress and perspectives on phononic crystals](#)

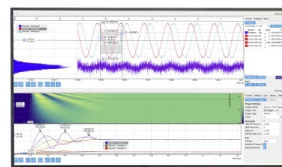
Journal of Applied Physics **129**, 160901 (2021); <https://doi.org/10.1063/5.0042337>

[Toward single-layer Janus crystals: Off-balance materials from synthesis to nanotechnology applications](#)

Journal of Applied Physics **129**, 160902 (2021); <https://doi.org/10.1063/5.0041054>

Challenge us.

What are your needs for periodic signal detection?



Zurich  
Instruments

# Determination of the temperature coefficient of resistance from micro four-point probe measurements

Cite as: J. Appl. Phys. **129**, 165105 (2021); doi: [10.1063/5.0046591](https://doi.org/10.1063/5.0046591)

Submitted: 4 February 2021 · Accepted: 8 April 2021 ·

Published Online: 27 April 2021



Thomas A. Marangoni,<sup>1,2</sup>  Benny Guralnik,<sup>1,3</sup>  Kasper A. Borup,<sup>4</sup>  Ole Hansen,<sup>5</sup>  and Dirch H. Petersen<sup>1,a)</sup> 

## AFFILIATIONS

<sup>1</sup>Department of Energy Conversion and Storage, Technical University of Denmark, Fysikvej, Building 310, DK-2800 Kgs. Lyngby, Denmark

<sup>2</sup>Department of Physics, Technical University of Denmark, Fysikvej, Building 307, DK-2800 Kgs. Lyngby, Denmark

<sup>3</sup>CAPRES—a KLA company, Diplomvej 373, 2800 Kgs. Lyngby, Denmark

<sup>4</sup>Department of Chemistry, Aarhus University, Langelandsgade 140, DK-8000 Aarhus C, Denmark

<sup>5</sup>National Centre for Nano Fabrication and Characterization, DTU Nanolab, Technical University of Denmark, DK-2800 Kgs. Lyngby, Denmark

<sup>a)</sup>Author to whom correspondence should be addressed: [dhpe@dtu.dk](mailto:dhpe@dtu.dk)

## ABSTRACT

Current characterization methods of the temperature coefficient of resistance (TCR) of thin films are often limited to slow macroscale measurements, which further require a direct determination of temperature. In this work, we present an innovative application of micro four-point probe (M4PP) sensing, which enables a fast, non-destructive, local measurement of Joule heating effects that can be translated into TCR of the thin film. Analytical expressions for the four-point resistance response to local heating, and ultimately the temperature profile during an M4PP measurement, are derived and validated against finite element models. The method is successfully demonstrated on three metal thin films (7, 10, and 16 nm platinum deposited on fused silica). We evaluate TCR using two different electrode configurations, resulting in unique temperature fields, and observe a measurement repeatability of <2% for each configuration. Furthermore, the M4PP-TCR method shows only a minor (~18%) systematic offset relative to reference TCR measurements obtained via an independent physical property measurement system. Our results demonstrate a new technique for characterizing TCR on the micrometer scale, adequately backed by theory. The measurement time is just a few seconds and could allow for thin film TCR mapping or in-line process monitoring on test structures.

© 2021 Author(s). All article content, except where otherwise noted, is licensed under a Creative Commons Attribution (CC BY) license (<http://creativecommons.org/licenses/by/4.0/>). <https://doi.org/10.1063/5.0046591>

## I. INTRODUCTION

The temperature coefficient of resistance (TCR) is a coefficient of a polynomial (typically linear) approximation of the fractional change in the electrical resistivity  $\rho$  of a material ( $d\rho/\rho$ ) upon an incremental change in temperature ( $dT$ ), validated and applicable within a certain thermal range.<sup>1</sup> Considering that the exact functional relationship  $\rho = f(T)$  depends on a multitude of material properties (e.g., geometry, grain size, chemical composition, defects and impurities, etc.), it becomes susceptible to mathematical description only for certain isolated effects, such as thin film

thickness<sup>2</sup> or semiconductor doping level.<sup>3</sup> TCR, on the other hand, is a phenomenological and straightforward experimental metric, obtained by fitting the fractional change in resistivity over a certain temperature range using a polynomial of temperature,<sup>4</sup> most often sufficiently well described by its linear part alone.<sup>1</sup> During the 19th and the early 20th centuries, the TCR of metals (positive, and generally falling within the 2–6‰ K<sup>-1</sup> range) received considerable attention from leading experimentalists including Lenz, Becquerel, Siemens, Clausius, Kirchhoff, and Matthiesen.<sup>5</sup> Following the boom of semiconductors and functional oxides after the Second World

War, materials with negative TCR have been discovered, documented, and heavily utilized in thermometry.<sup>6</sup> Most recent advances of the past decade include the fabrication of zero-TCR<sup>7,8</sup> or tunable-TCR materials.<sup>9,10</sup>

Today, the TCR has a wide range of applications in microelectronics and material and device characterization. Tunable or zero TCR materials such as antiperovskite compounds<sup>7–10</sup> are desirable in reference resistors and anti-surge resistors in high power applications. In addition, zero- to low-TCR conductors are beneficial in limiting the effects of self-heating of micro- and nanoelectronic devices which, in turn, promotes low energy-consumption electronics.<sup>11,12</sup> The characterization of the resistance and cross-sectional area<sup>13,14</sup> as well as the reliability and performance of interconnects<sup>15,16</sup> can be achieved via measurements of TCR. A precise knowledge of TCR is also essential in the fabrication of, e.g., thermal<sup>17</sup> and flow<sup>18</sup> sensors. In addition, TCR can be applied to determine doping levels in silicon-based resistors.<sup>3</sup> Thus, both the engineering and the post-fabrication determination of TCR remain an extremely relevant and active field of research, as thermal effects start bringing Moore's law to a stall.<sup>19</sup>

As materials are scaled down to nanometer dimensions, the TCR deviates from its bulk value. This deviation is predicted by an adaptation of the Mayadas–Schatzkes model of thin film resistivity<sup>2,20</sup> and observed in nanometer thin films.<sup>21–25</sup> Current techniques for characterizing TCR are limited to measuring patterned thin film resistors<sup>22,26,27</sup> and additionally require a separate, independent temperature measurement. This could be in the form of a temperature controlled chamber,<sup>22</sup> keeping the entire sample at an equilibrium temperature. Alternatively, one can locally measure the temperature during a resistance measurement via a fabricated thermocouple near the points of interest.<sup>28</sup> While this does encompass self-heating and local effects, it requires the need for complex sample preparation.

In this work, we present a method capable of locally measuring the TCR of ultrathin conductive films without requiring a separate temperature measurement by utilizing a by-product of four-terminal sensing, namely, Joule heating. The micro four-point probe (M4PP)<sup>29</sup> is a widely used metrology for the characterization of metallic and semiconducting thin films, including magnetic

tunnel junctions<sup>30</sup> and ultrashallow junctions.<sup>31</sup> Sheet resistance of thin films<sup>32,33</sup> can be rapidly measured with high precision,<sup>34</sup> and it is possible to measure accurately in small test pads down to  $10 \times 10 \mu\text{m}^2$ <sup>35,36</sup> or perform entire wafer scans.<sup>37</sup> It is even possible to measure the line resistance on fins down to 20 nm width.<sup>38,39</sup> So far, Joule heating in M4PP has been perceived as a problem and addressed primarily via minimization strategies.<sup>40,41</sup> Conversely, in this study, we instead amplify Joule heating and utilize it to constrain important material properties previously unaddressed by a M4PP measurement setup.

## II. THEORY

### A. Transfer resistance of a thin film obeying a linearized resistivity model

During a four-point probe measurement, current  $I$  flows through a material with resistivity  $\rho$ , from the current source electrode located at  $\mathbf{r}_+$  to the drain electrode at  $\mathbf{r}_-$ , while the resulting potential difference is being sensed across two other electrodes located at  $\mathbf{r}_{V+}$  and  $\mathbf{r}_{V-}$ . In this work, we focus on the current distribution in an “infinitely thin” conductive sheet (e.g., a metallic thin film), whose thickness  $d$  is negligible in comparison to all other distances considered [Fig. 1(a)]. For convenience, electric resistivity and film thickness are herewith combined into the sheet resistance  $R_S = \rho/d$ .

During the measurement, the electric sheet current density  $\mathbf{J}_S$  at an arbitrary location  $\mathbf{r}$  on the sheet may be obtained via a superposition of the radial current densities around the source and drain electrodes, respectively,

$$\mathbf{J}_S(\mathbf{r}) = \frac{I(\mathbf{r} - \mathbf{r}_+)}{2\pi|\mathbf{r} - \mathbf{r}_+|^2} + \frac{-I(\mathbf{r} - \mathbf{r}_-)}{2\pi|\mathbf{r} - \mathbf{r}_-|^2}. \quad (1)$$

Consequently, the sheet power density at  $\mathbf{r}$  is given by

$$R_S(\mathbf{r})|\mathbf{J}_S(\mathbf{r})|^2 = \frac{R_S(\mathbf{r})I^2}{4\pi^2} \left( \frac{|\mathbf{r}_+ - \mathbf{r}_-|}{|\mathbf{r} - \mathbf{r}_+||\mathbf{r} - \mathbf{r}_-|} \right)^2, \quad (2)$$

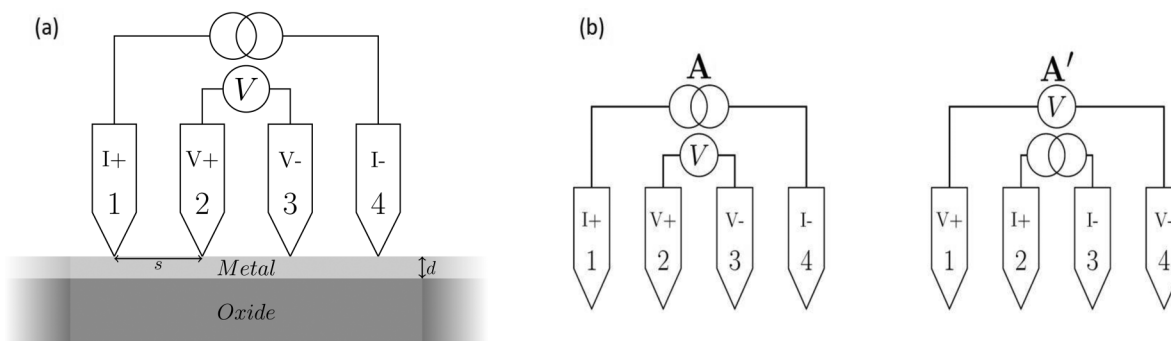


**FIG. 1.** (a) Schematic of a collinear and equidistant micro four-point probe, in contact with a thin metal film deposited onto a thick oxide. (b) Two specific configurations of current and voltage assignment (A and A') were utilized for numerical simulations and actual measurements. I+ and I- denote the current injection and extraction electrodes, respectively, while V+ and V- indicate the voltage probing electrodes and their polarities. A' is considered as the adjoint configuration of A (and vice versa), since it is obtained by swapping of the current and voltage assignments (see text).

where  $R_S(\mathbf{r})$  is the local sheet resistance, and the bracketed fraction is the source-to-drain distance further divided by the separation distances of  $\mathbf{r}$  from both the source and the drain.

Joule heating, defined to be proportional to the power in Eq. (2), causes a local change in the surface temperature  $\Delta T(\mathbf{r})$  and thereby a local change in  $R_S(\mathbf{r})$ , which under a linear TCR approximation<sup>42</sup> is given by

$$R_S(\mathbf{r}) = R_{S,0}[1 + \alpha_{\text{TCR}}\Delta T(\mathbf{r})], \quad (3)$$

where  $\alpha_{\text{TCR}}$  is the temperature coefficient of resistance and  $R_{S,0}$  is the sheet resistance at a reference temperature  $T_0$  (relative to which  $\Delta T = T - T_0$  is evaluated).

To predict how the behavior of a system obeying Eqs. (1)–(3) is reflected in M4PP measurements, we start by considering the case of  $\alpha_{\text{TCR}} = 0$  leading to a spatially uniform  $R_S(\mathbf{r}) = R_S$ . The potential drop  $\Delta V$  measured across the voltage pins divided by the current is known as “transfer resistance”  $R = \Delta V/I$  and is given by

$$R = \frac{R_S}{F}, \quad F = 2\pi / \ln\left(\frac{|\mathbf{r}_+ - \mathbf{r}_{V-}| |\mathbf{r}_- - \mathbf{r}_{V+}|}{|\mathbf{r}_+ - \mathbf{r}_{V+}| |\mathbf{r}_- - \mathbf{r}_{V-}|}\right), \quad (4)$$

where  $F$  is a transfer function, depending on four inter-electrode separation distances.<sup>32,43</sup> To generalize Eq. (4) for  $\alpha_{\text{TCR}} > 0$  where  $R_S(\mathbf{r})$  becomes non-uniform, we replace  $R_S$  with a spatial integral of  $R_S(\mathbf{r})$  according to Koon *et al.*,<sup>43</sup>

$$R = \frac{\int_{\Omega} R_S(\mathbf{r}) \hat{S}(\mathbf{r}) d\Omega}{F}, \quad \hat{S}(\mathbf{r}) = \frac{\mathbf{J}_S(\mathbf{r}) \cdot \tilde{\mathbf{J}}_S(\mathbf{r})}{\int_{\Omega} [\mathbf{J}_S(\mathbf{r}) \cdot \tilde{\mathbf{J}}_S(\mathbf{r})] d\Omega}, \quad (5)$$

where  $\Omega$  is the area of the sheet,  $d\Omega$  its infinitesimal element, and  $\hat{S}(\mathbf{r})$  is the M4PP sensitivity to a local perturbation at  $\mathbf{r}$ . From Eq. (5), it is clear that  $\hat{S}(\mathbf{r})$  acts as a spatial weighting function with units of ( $\text{m}^{-2}$ ) (cf. Ref. 43, who further nondimensionalized  $\hat{S}$  through multiplication by an arbitrary area). The weights in  $\hat{S}$  magnify or suppress the effect of local  $R_S$  variations on the resultant single value of  $R$  according to the dot product between  $\mathbf{J}_S$ , the actual current density in the system [Eq. (1)], and  $\tilde{\mathbf{J}}_S$ , the hypothetical current density in an adjoint system with interchanged current and voltage assignments<sup>44</sup> [e.g.,  $\mathbf{J}_{S,A} = \mathbf{J}_{S,A'}$  and  $\tilde{\mathbf{J}}_{S,A'} = \mathbf{J}_{S,A}$  in Fig. 1 (b)].

Combining Eqs. (3) and (5), we can express the fractional change in the M4PP transfer resistance as

$$\frac{R - R_0}{R_0} = \alpha_{\text{TCR}} \int_{\Omega} \Delta T(\mathbf{r}) \hat{S}(\mathbf{r}) d\Omega, \quad (6)$$

where  $R_0$  is the “zero-current resistance,”<sup>45</sup> i.e., its idealized value unaffected by Joule heating.

## B. Calculation of the temperature profile in a thin film blanket

To put Eq. (6) into practice, we proceed to consider a thin film “blanket,” e.g., a thin layer of metal deposited onto an “infinitely thick” and electrically inert substrate. We expect the thermal resistance of the system to be dominated by the thermal

conductivity  $\kappa$  of the substrate. Thus, for simplicity, we neglect lateral heat transport through the thin film and the thermal loss to air. We further assume Peltier heat displacement is negligible.

We will divide the sheet into two distinct regions, namely, the contact areas under the current source and drain, and all the remaining areas outside of both contacts. We can approximate the contact geometry under the current electrodes as circular disks of radius  $r_0$ , and define that all the resistance at distances  $r < r_0$  (including contribution from contact resistivity and spreading resistance) contributes to the “contact resistance”  $R_+$  and  $R_-$ , at the current source and drain respectively (for calculation of  $R_+$  and  $R_-$ , from two terminal resistance data, see Appendix A). Consequently, these contact areas will be excluded from Eq. (2). The Joule heat produced by  $R_+$  and  $R_-$  at  $\mathbf{r}_+$  and  $\mathbf{r}_-$ , respectively, can be modeled as a point heat source. Solving for heat diffusion from a point source into a bulk half-space,<sup>46</sup> the temperature rise at an arbitrary location  $\mathbf{r}$  should obey

$$\Delta T_{\text{contacts}}(\mathbf{r}) = \frac{I^2 R_+}{2\pi\kappa} \frac{1}{|\mathbf{r} - \mathbf{r}_+|} + \frac{I^2 R_-}{2\pi\kappa} \frac{1}{|\mathbf{r} - \mathbf{r}_-|}. \quad (7)$$

Treating the sheet power density [Eq. (2)] as a continuous distribution of point heat sources yields a similar expression,

$$\Delta T_{\text{sheet}}(\mathbf{r}) = \int_{\mathbf{r}' \in \Omega} \frac{R_S(\mathbf{r}') |\mathbf{J}_S(\mathbf{r}')|^2}{2\pi\kappa} \frac{d\Omega}{|\mathbf{r} - \mathbf{r}'|}, \quad (8)$$

where  $\mathbf{r}'$  is an arbitrary location where the sheet power density is  $R_S(\mathbf{r}') |\mathbf{J}_S(\mathbf{r}')|^2$  according to Eq. (2), and  $d\Omega$  is its corresponding infinitesimal area. The total temperature change at an arbitrary location  $\mathbf{r}$  is then the sum of Eqs. (7) and (8), with  $R_S(\mathbf{r}')$  further substituted from Eq. (3),

$$\Delta T(\mathbf{r}) = \frac{I^2}{2\pi\kappa} \left( \frac{R_+}{|\mathbf{r} - \mathbf{r}_+|} + \frac{R_-}{|\mathbf{r} - \mathbf{r}_-|} + \frac{R_{S,0} |\mathbf{r}_+ - \mathbf{r}_-|^2}{4\pi^2} \int_{\mathbf{r}' \in \Omega} \frac{1 + \alpha_{\text{TCR}} \Delta T(\mathbf{r}')}{|\mathbf{r}' - \mathbf{r}_+|^2 |\mathbf{r}' - \mathbf{r}_-|^2 |\mathbf{r}' - \mathbf{r}|} d\Omega \right). \quad (9)$$

Note that Eq. (9) is implicit with regard to  $\Delta T$ , arising from the circular dependence of the sheet resistance on temperature in the TCR definition [Eq. (3)], and of temperature on sheet resistance in the Joule heating [Eqs. (2) and (8)]. Despite the recursion, Eq. (9) does rapidly converge for a broad range of realistic values [typically within 3 iterations for an initial guess of  $\Delta T = 0$  and  $R_S(\mathbf{r}) = R_S$ ]. Since the contact areas are negligible, the contact resistances  $R_+$  and  $R_-$  are assumed to be constant, i.e., independent of current and temperature; relaxing this assumption leads to practically unaltered results, on the expense of another level of implicitness for  $\Delta T$ , i.e.,  $R_{\pm} = f(I, \Delta T)$ .

## C. Practical considerations

The treatment in Secs. II A and II B has been developed and numerically validated for an arbitrary M4PP pin configuration, applicable as long as its relevant current distributions (self  $\mathbf{J}_S$  and adjoint  $\tilde{\mathbf{J}}_S$ ) can be calculated. Hereafter, we proceed to focus on

only two collinear and equidistant pin configurations A and A' [Fig. 1(b)], whose induced current flow in the sample, and thus the heat generation and resulting temperature distribution, are markedly different [Figs. 2(a) and 2(b), respectively]. However, since A and A' are mutually adjoint configurations [Fig. 1(b)], they both share the same sensitivity function [ $\hat{S}$  in Eq. (5)], depicted in Fig. 2(c). This shared sensitivity allows us to attribute any deviations of the observed resistance  $R$  from zero-current resistance  $R_0$  to thermal effects only [cf. Eq. (6)]. Additionally, the symmetry of both configurations about the probe center makes them

significantly less sensitive to variation in contact resistance ( $R_{\pm}$ ) across the four probe pins [cf. Eq. (9)].

Finite element simulations of the temperature rise  $\Delta T(\mathbf{r})$ , associated with a M4PP measurement of a  $R_S = 14.4 \Omega$  thin film with a DC current of 5 mA under configurations A and A', are shown in Figs. 2(a) and 2(b), respectively (probe pitch  $10 \mu\text{m}$ ,  $\alpha_{\text{TCR}} = 2 \times 10^{-3} \text{K}^{-1}$ ,  $R_{\pm} = 0 \Omega$ ). Figure 2(c) shows the associated sensitivity function, common to both A and A'. The areas of positive (negative) sensitivity imply an increase (decrease) in the measured transfer resistance  $R$ , given a local increase in  $R_S$  due to a positive TCR. From a qualitative study of Fig. 2, we may expect a higher increase in  $R$  in the A' configuration, since more of the heated area is concentrated within a region of positive sensitivity  $\hat{S}(\mathbf{r}) > 0$ .

### III. METHODS

#### A. Materials and instrumentation

Three metal-on-insulator thin films were fabricated by e-beam evaporation as follows. The substrate of all samples consisted of a 1 mm thick and double side polished 4-inch wafer of fused silica, chosen to serve two purposes: to restrict Joule heating solely to the thin film, and to magnify the resultant thermal gradients (given its low thermal conductivity, presumed to be  $1.4 \text{W m}^{-1} \text{K}^{-1}$ ). An adhesion layer of 1 nm Ti, followed by a platinum thin film of a desired thickness, was deposited on one side of the wafer via e-beam evaporation (Wordentec QCL800). A total of three samples, with nominal Pt film thicknesses of 7, 10, or 16 nm, were fabricated (the observed non-uniformity of the 10 nm thin film may be attributed to a broken vacuum seal during its fabrication). The fabricated wafers were subsequently split into smaller coupons, up to  $11 \times 14 \text{mm}$  in size.

To obtain an independent estimate of the TCR, several coupons of each wafer (Table I) were measured using a physical property measurement system (PPMS from Quantum Design). For those measurements, the surface of the platinum thin film was contacted at four locations at the coupon's edges, allowing for a four-terminal measurement of the film's resistance. The sample was then placed in a temperature controlled chamber, where temperature was ramped from 290 to 310 K in steps of 5 K, while the resistance being continuously measured using an AC current with  $I_{\text{RMS}} = 5 \text{mA}$  at  $f = 18.3 \text{Hz}$ . To obtain the TCR at room temperature (293 K),  $R = R_0[1 + \alpha_{\text{TCR}}\Delta T]$  [cf. Eq. (3)] was directly fitted to the paired  $T$  and  $R$  data.

The M4PP measurements were performed on a microRSP A300 system from CAPRES A/S, which measures the resistance using a lock-in amplifier. We used a collinear seven-point probe with equidistant  $10 \mu\text{m}$  pitch.<sup>47</sup> The polysilicon electrodes were coated with a 100 nm Ni layer serving as the current carrier. After the probe is brought into physical contact with the sample surface, electric measurements proceed at user-selected currents and pin configurations. For reproducibility, we performed up to 30 consecutive engages, laterally spaced apart by  $20 \mu\text{m}$ . At each engagement, an AC current at  $f = 12.055 \text{Hz}$  is forced through the sample while switching through several electrode configurations, including the aforementioned A and A' configurations (Sec. II C). During each engagement, the AC current was ramped from  $I_{\text{RMS}} = 5 \text{mA}$  down to 0.5 mA in seven steps, and ramped up again for three replicate

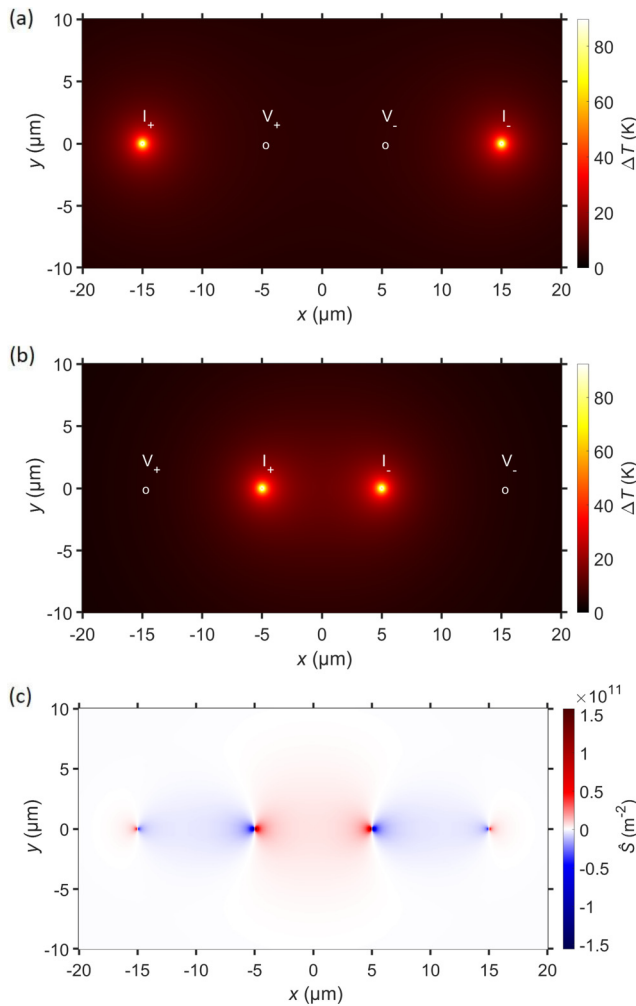


**FIG. 2.** (a) The surface temperature increase generated during a 5 mA M4PP measurement on a 16 nm platinum film in the A configuration, obtained from a finite element simulation with  $R_S = 14.4 \Omega$ ,  $\alpha_{\text{TCR}} = 2 \times 10^{-3} \text{K}^{-1}$  and no contact resistance. The locations of the voltage electrodes are indicated. (b) The surface temperature increase, obtained from an identical finite element simulation with the probe in the A' configuration, with the locations of the voltage electrodes indicated. (c) The calculated probe sensitivity for this probe, valid for both the A and A' configurations.

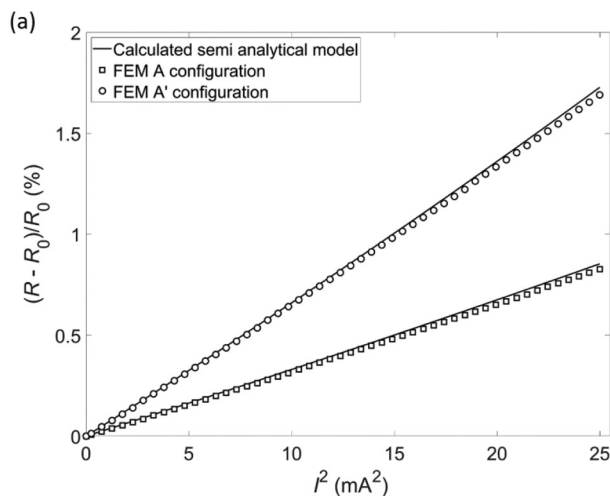
measurements. The potential drop across the voltage electrodes  $V$  is measured with a lock-in amplifier and reported as transfer resistance  $R = V/I_{\text{RMS}}$ . The corresponding sheet resistance is calculated using the dual configuration method.<sup>48</sup>

To calibrate lead resistances and monitor potential drift in contact resistances, a reference M4PP measurement on a thick nickel slab is performed before and after every group of ten measurements on the samples. The reference measurement frequency, pin configurations and currents are identical to an engage on a real sample; given that the  $R_S = 0.48 \Omega$  of the Ni reference is by  $\sim 2$  orders of magnitude lower than that of the studied samples, we evaluate the two-point resistance of the calibration measurements as dominated by the lead resistance, that is, the contribution from all sample-unrelated sources (following all the interconnects from the electrode cantilevers up to the current generator). This lead resistance is then subtracted from measurements made on the Pt thin films<sup>49</sup> (the calculation of contact resistances is detailed in Appendix A).

## B. Numerical approach

To extract the TCR from M4PP resistance measurements on the microRSP A300 as described in Sec. III A, Eq. (6) has to be adapted to AC currents, and solved. The adaptation to AC currents is straightforward (Appendix B), scaling the solution by a constant  $c = 3/2$ . However, since the integral in Eq. (6) does not appear amenable to a closed-form solution, a semi-analytical approach was adopted, namely, evaluating an adapted Eq. (6) over a mesh of  $n$  finite elements,

$$\frac{dR}{R} \cong \frac{R - R_0}{R_0} = c\alpha_{\text{TCR}} \sum_{i=1}^n \Delta T(\mathbf{r}_i) \hat{S}(\mathbf{r}_i) \Omega_i, \quad (10)$$



where  $c = 3/2$  is the AC prefactor (Appendix B),  $\mathbf{r}_i$  is the centroid of a mesh element  $i$ , and  $\Omega_i$  the corresponding element's area. After testing several straightforward implementations (including densely meshed regular grids, quad-trees,<sup>50</sup> and DistMesh,<sup>51</sup> the best tradeoff between computational time and calculation accuracy was achieved by constructing a specialized mesh as follows. For each configuration, each of the theoretically circular electrode contacts at  $\mathbf{r}_+$ ,  $\mathbf{r}_-$ ,  $\mathbf{r}_{V+}$ , and  $\mathbf{r}_{V-}$  is approximated as an 18-sided hollow regular polygon; the rest of the mesh is constructed by the advancing front technique, i.e., via concentric polygons at geometrically progressing radii (growth rate of 1.08), which are triangulated to existing nodes at each incremental step. The outer extent of the mesh, determined by the condition  $\int_{\Omega} [\mathbf{J}_S(\mathbf{r}_i) \cdot \tilde{\mathbf{J}}_S(\mathbf{r}_i)] d\Omega \cong (I/2\pi)^2$ , was practically achieved (to within 0.01%) by reaching a perimeter that is three times the probe footprint (maximum inter-electrode distance) away from the probe's center. To further increase the performance by twofold, (anti)symmetric triangles sharing a long side were merged into quadrangles, leaving only  $\sim 1\%$  of patching triangles at points of irregularity (convergence of arcs belonging to different centers). The final mesh typically contains a few thousand elements. For each element, the sensitivity  $[\hat{S}(\mathbf{r}_i)]$  via Eq. (5) must be pre-calculated only once, while three iterations of temperature  $[\Delta T(\mathbf{r}_i)]$  via Eq. (10) per a given current, converge to a stable value on the sub-second timescale.

## IV. RESULTS

The results of the semi-analytical model [Eq. (10)] were benchmarked against a matching finite element model (FEM) implemented in COMSOL Multiphysics,<sup>52</sup> simulating M4PP measurements in the 0.5–5 mA range (DC) on a conductive thin film with a TCR value of  $2\% \text{K}^{-1}$  (probe pitch of  $10 \mu\text{m}$  and contact radii of  $r_0 = 100 \text{nm}$ ). The COMSOL model takes advantage of the

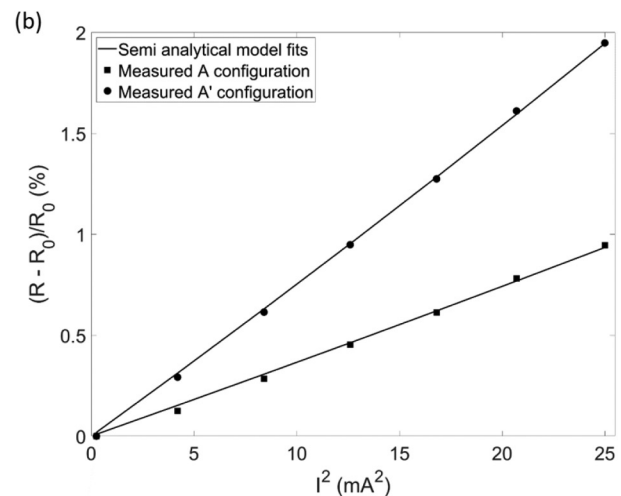


**FIG. 3.** (a) The increase in resistance given by the DC semi-analytical model [Eq. (10) with  $c = 1$ ] and finite element simulations (FEM) of both the A and A' configurations, on the same simulated 16 nm Pt film with the same arbitrary TCR value. (b) The AC semi-analytical model [Eq. (10) with  $c = 3/2$ ] fit to measured data taken on a 16 nm Pt film for both the A and A' configurations with a probe pitch of  $10 \mu\text{m}$ . The measured data shown is the mean value over 20 engagements with the error bars inside the symbols. The semi-analytical model is shown as a continuous line corresponding to calculated resistance values using the TCR obtained from the nonlinear least square fit.

**TABLE I.** Overview of all TCR values compared to the reference values measured via PPMS on the same films. The TCR is extracted on each sample separately for the A and A' configurations, all measured on the same probe with a pitch of  $10\ \mu\text{m}$ . The M4PP values show the standard error, while the PPMS carries a 5% measurement error.

Nominal thin film thickness (nm)	Coupon ID	Sheet resistance ( $\Omega$ )	Temperature coefficient of resistance ( $10^{-3}\ \text{K}^{-1}$ )		
			M4PP A	M4PP A'	PPMS (cm-scale)
7	Pt-7nm-b	50.59	$0.73 \pm 0.01$	$0.76 \pm 0.01$	$0.96 \pm 0.05$
	Pt-7nm-c	50.40	$0.74 \pm 0.01$	$0.74 \pm 0.01$	$0.97 \pm 0.05$
10	Pt-10nm-a	28.05	$1.13 \pm 0.02$	$1.17 \pm 0.01$	$1.38 \pm 0.07$
	Pt-10nm-b	24.05	$1.34 \pm 0.02$	$1.40 \pm 0.01$	$1.60 \pm 0.08$
16	Pt-16nm-a	14.55	$1.59 \pm 0.03$	$1.63 \pm 0.01$	$1.71 \pm 0.09$
	Pt-16nm-c	14.48	$1.58 \pm 0.02$	$1.63 \pm 0.01$	$1.77 \pm 0.09$

“heat transfer in solids” module for the substrate, and “electric currents in shells” module for the metallic thin film, linked through the “electromagnetic heating multiphysics.” The sample was represented by an  $800 \times 800 \times 400\ \mu\text{m}$  square of fused silica with a thin, electrically conductive shell at its top boundary, the latter further assigned a linearized resistance model [Eq. (3)], with a room temperature sheet resistance  $R_{S,0}$  equivalent to a 16 nm Pt film. Centered on the top boundary, the M4PP was modeled as four equidistantly placed circles serving as the electrode contacts, with a DC current injected at the perimeter of the I+ contact, and extracted at the perimeter of the I- contact. The induced voltage was measured at the center of the two voltage electrode contacts, mimicking the M4PP voltage measurement.

The predicted fractional change in the measured transfer resistance  $dR/R \cong (R - R_0)/R_0$  for the considered configurations (A/A'), as calculated using the semianalytical [solid lines in Fig. 3(a)] and the FEM approach [“□”/“○” in Fig. 3(a)], shows acceptable agreement (<1%) over a broad range of currents, thus validating the use of Eq. (10) for data reduction of actual measurements [Fig. 3(b)].

The results of all PPMS and M4PP measurements on the three samples (2 coupons per sample) are listed in Table I and summarized in Fig. 4. The derivation of each particular TCR is further exemplified in Fig. 3(b), showing experimental data for the Pt-16nm-c coupon, and the best-fit semianalytical model [Eq. (10)] for configurations A and A'. These fits were obtained via a nonlinear least square optimization of multiple instances of Eq. (10) for different currents, assuming a shared  $\alpha_{\text{TCR}}$ . To avoid bias (mixing of different thermal fields), configurations A and A' are fitted separately. The observed increase in  $dR/R$  with respect to  $I^2$  is overwhelmingly linear, as expected from the linearized resistivity model. Equally linear plots of  $dR/R$  vs  $I^2$  were observed also for the two thinner samples. The data are reproducible across dozens of M4PP engages, with a relative standard deviation of 1%–3% for all currents  $\geq 2\ \text{mA}$ . In terms of signal to noise ratio, the TCR “signal” ( $R - R_0$ ) is up to 2% of  $R$  at the highest current; given typical associated electrical noise at the 0.1% level, we conclude that TCR effects are most readily detectable by M4PP.

Estimates of TCR from M4PP data are compared to direct measurements of TCR using PPMS in Table I and Fig. 4. Both methods indicate a decrease in TCR for thinner films, as predicted by the Mayadas–Schatzkes theory and previously documented

elsewhere.<sup>2,22</sup> The TCRs from A configurations are marginally lower than those from the A' configurations (by up to 4%); in turn, both configuration underestimate the independent PPMS measurements by  $\sim 18\%$  (discussed in detail in Sec. V). Despite such underestimations, seen at large, the two independent datasets PPMS and M4PP are strikingly correlated (a Pearson's correlation coefficient of 0.99), and pave a promising route for the application of M4PP to TCR monitoring. Initially perceived as an obstacle, the low homogeneity of the 10 nm thin film (“□” symbols in Fig. 4), serves well for methodological intercomparison, as the minor variance in TCR across two coupons of the same sample is perfectly correlated across the two methods, suggesting that the presented

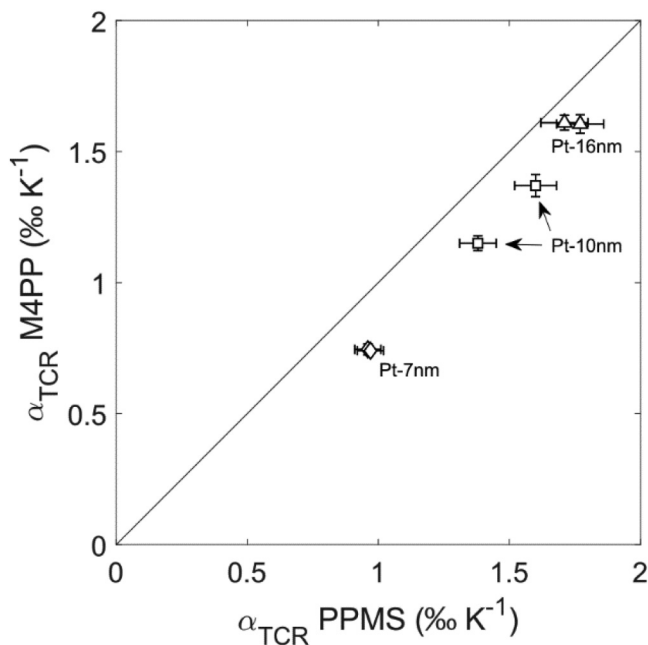


**FIG. 4.** The TCR obtained via the from the M4PP-TCR method compared to independent reference measurements performed on a PPMS on a total of six coupons taken from the three samples with varying platinum film thickness. During the fabrication of the 10 nm sample, the vacuum seal was broken.



M4PP methodology is at least as sensitive as direct TCR measurements with PPMS.

## V. DISCUSSION AND CONCLUSION

To address the M4PP underestimation of  $\alpha_{\text{TCR}} = dR/RdT$  relative to PPMS, we stress that since M4PP is extremely precise ( $<0.1\%$ )<sup>34</sup> in measuring resistance and thus resistance differences ( $dR$  and  $R$ ), the most straightforward reason for the underestimation is that our model overestimates the effective  $dT$ . To this end, the thermal model in Secs. II A and II B is certainly incomplete, and we can try to evaluate which critical parts are missing. While thermoelectric effects (primarily Peltier heat) have been neglected, their contribution to temperature is expected to be minimal, as the Seebeck coefficient of bulk Pt is only around  $-5 \mu\text{V K}^{-1}$ .<sup>53</sup> Second, a “cold finger” effect, i.e., heat dissipation through the electrodes rather than the substrate, could be in place, for which the theory does not account either. Third, ignoring heat transfer through the thin film builds up local thermal gradients which would otherwise be dissipated away.

While all of the above effects might need closer inspection, it is our impression that the key contributor to temperature overestimation is a time delay between the instantaneous heat generation at a location  $\mathbf{r}'$ , and its arrival at another arbitrary location  $\mathbf{r}$ , resulting in a temperature distribution that is slightly out of phase from the one calculated in Eq. (9).

This work has demonstrated that four-terminal sensing at micrometer scale can induce significant and measurable Joule heating effects, which under favorable measurement conditions, reasonable assumptions, and theoretical approximations can be converted into relatively accurate TCR estimates of ultrathin metal films. Both the advantage and the disadvantage of the presented method are that it requires no external temperature measurement, as the temperature is estimated directly from Joule heating, alongside assumptions about the sample's geometry and thermal conductivity. If the latter are reasonably known, M4PP applications require no sample preparation (*in situ* measurements), impose minimal sample damage, are extremely rapid (10 s per measurement), and capable of highly precise resistance measurements ( $<0.1\%$ ). The drawback of the method, as evident from Eq. (9), is that an external assumption must be made about the thermal conductivity (thermal resistance) of the thin film's substrate, which may become progressively difficult when multilayered substrates are considered. One possible solution to bypass the uncertainties that go into the thermal modeling is by scaling the observed  $dR/R$  trends by power (instead of temperature), and reporting the best-fit slopes as the “Power Coefficient of Resistance” (PCR), which is a useful metric for the estimation of self-heating of high precision electronics and interconnects.<sup>54–56</sup> However, given the apparent definition fluidity whether PCR does or does not include the TCR effect, we currently prefer that our method be labeled as “TCR estimation,” rather than “PCR measurement.”

We believe that the presented methodology opens a new portfolio of M4PP applications, enabling the characterization of thin film TCR and their spatial variance at unprecedented spatial scales. Although this study is limited to homogenous platinum thin films, we expect that the method can be extended to semiconductor thin

films by taking into account thermoelectric properties and non-ohmic contacts.

## ACKNOWLEDGMENTS

This work has been supported by the Innovation Fund Denmark (Grant Nos. 8054-00020B and 8057-00010B) and the Sapere Aude (Independent Research Fund Denmark) (No. 8048-00088B). We thank Frederik W. Østerberg, Henrik H. Henrichsen, and Peter F. Nielsen of CAPRES A/S and Bo B. Iversen of Aarhus University with their valuable input.

## APPENDIX A: CALCULATION OF CONTACT RESISTANCE ON A THIN SHEET

The two-point resistance  $R_{\text{load},ij}$  measured during a M4PP measurement between electrode pins  $i$  and  $j$  corresponds to the in-series (sum) resistance of the sample  $R_{\text{samp},ij}$ , the contact resistances  $R_{c,i}$  and  $R_{c,j}$  in the proximity of each electrode-sample interface, and the lead resistances  $R_{\text{lead},i}$  and  $R_{\text{lead},j}$  within the electrodes themselves and all the interconnects up to the voltmeter,

$$R_{\text{load},ij} = R_{\text{samp},ij} + R_{c,i} + R_{c,j} + R_{\text{lead},i} + R_{\text{lead},j}. \quad (\text{A1})$$

The sample resistance  $R_{\text{samp},ij} = \frac{R_{s,0}}{\pi} \text{arccosh}\left(\frac{D_{ij}}{2r_0}\right)$ , where  $D_{ij}$  is the electrode separation distance.<sup>49</sup> In Eq. (A1),  $R_{\text{load},ij}$  is a measured value, while lead resistances  $R_{\text{lead},i}$  and  $R_{\text{lead},j}$  are known from the probe design (and can be further validated via measurements on highly conductive substrates). Writing  $\tilde{R}_{ij} = R_{\text{load},ij} - R_{\text{lead},i} - R_{\text{lead},j} - R_{\text{samp},ij}$  leaves only  $R_{c,i}$  and  $R_{c,j}$  as unknowns, which can be determined via three measurements,

$$\begin{aligned} \tilde{R}_{1,2} &= R_{c,1} + R_{c,2}, \\ \tilde{R}_{1,3} &= R_{c,1} + R_{c,3}, \\ \tilde{R}_{2,3} &= R_{c,2} + R_{c,3}, \end{aligned} \quad (\text{A2})$$

which can be linearly combined to yield

$$R_{c,1} = \frac{\tilde{R}_{1,2} + \tilde{R}_{1,3} - \tilde{R}_{2,3}}{2}, \quad (\text{A3})$$

and analogously for  $R_{c,2}$  and  $R_{c,3}$ . This well-known approach<sup>57</sup> may be generalized for  $n$  two-point resistance measurements utilizing a total of  $m$  electrodes as follows. Let us write Eq. (A1) in matrix form as

$$R_c = (M^T M)^{-1} M^T (R_{\text{load}} - R_{\text{samp}} - M R_{\text{lead}}), \quad (\text{A4})$$

where  $R_{\text{load}}$  and  $R_{\text{samp}}$  are column vectors  $n \times 1$ , containing the observed load resistance, and the estimated sample resistance, and  $R_c$  and  $R_{\text{lead}}$  are row vectors  $1 \times m$ , containing the contact resistance of each electrode (to be solved for), and its lead resistance. The sparse matrix  $M$  consists of  $n$  rows (each representing a certain measurement configuration) and  $m$  columns (two of which are flagged as 1, marking the current electrodes, all the rest being 0).

Equation (A4) can be solved if the number of independent observations is equal or higher to the number of unknowns.

## APPENDIX B: ADAPTATION OF THE SEMIANALYTICAL MODEL TO ALTERNATING CURRENTS

Let us rewrite Eq. (6) in terms of voltage,

$$V = IR_0(1 + \alpha_{\text{TCR}}\Delta T_{\text{eff}}), \quad (\text{B1})$$

where  $\Delta T_{\text{eff}} = \int_{\Omega} \Delta T(\mathbf{r})\hat{S}(\mathbf{r})d\Omega$  is an effective temperature change. Despite the implicit form of  $\Delta T(\mathbf{r})$  in Eq. (9), its dependence on  $I^2$  is explicit from the definition of Joule heating, thus enabling us to write

$$\Delta T_{\text{eff}} = \theta P = \theta R_{\text{eff}}I^2, \quad (\text{B2})$$

where  $P$  is the applied power,  $\theta$  is the thermal resistance of the system and,  $R_{\text{eff}}$  is the effective resistance of the system. Let  $I$  be a sinusoidal current with amplitude  $I_0$  and angular frequency  $\omega$ ,

$$I = I_0 \cos(\omega t) = \sqrt{2}I_{\text{RMS}} \cos(\omega t). \quad (\text{B3})$$

Combining Eqs. (B1)–(B3), one has

$$V = R_0[I_0 \cos(\omega t) + \alpha_{\text{TCR}}\theta R_{\text{eff}}I_0^3 \cos^3(\omega t)]. \quad (\text{B4})$$

Considering the substitution  $I_0 = \sqrt{2}I_{\text{RMS}}$ , the identity  $\cos^3(x) = [\frac{3}{4}\cos(x) + \frac{1}{4}\cos(3x)]$ , and that the lock-in amplifier extracts the voltage only at the measurement frequency  $\omega$ , the root mean square voltage extracted at  $\omega$  is

$$V_{\text{RMS},1\omega} = R_0I_{\text{RMS}} \left( 1 + \frac{3}{2}\alpha_{\text{TCR}}\theta R_{\text{eff}}I_{\text{RMS}}^2 \right), \quad (\text{B5})$$

which differs by a factor 3/2 from Eq. (9), given the replacement  $\theta R_{\text{eff}}I_{\text{RMS}}^2 = \int_{\Omega} \Delta T(\mathbf{r})\hat{S}(\mathbf{r})d\Omega$ , and that four-point transfer resistances are reported as  $R = V_{\text{RMS},1\omega}/I_{\text{RMS}}$  by the CAPRES microRSP A300.

## DATA AVAILABILITY

The data that support the findings of this study are available from the corresponding author upon reasonable request.

## REFERENCES

- H. A. Schafft and J. S. Suehle, *Solid State Electron.* **35**, 403 (1992).
- C. Tellier, A. Tossier, and C. Boutrix, *Thin Solid Films* **44**, 201 (1977).
- M. Olszacki, C. Maj, M. Al Bahri, J. Marrot, A. Boukabache, P. Pons, and A. Napieralski, *J. Micromech. Microeng.* **20**(6), 064008 (2010).
- F. Kerrou, A. Boukabache, and P. Pons, *J. Sens. Technol.* **2**, 132 (2012).
- S. Reif-Acherman, *Rev. Bras. Ensino Fis.* **33**, 4602 (2011).
- A. Feteira, *J. Am. Ceram. Soc.* **92**, 967 (2009).
- L. Ding, C. Wang, L. Chu, J. Yan, Y. Na, Q. Huang, and X. Chen, *Appl. Phys. Lett.* **99**(25), 251905 (2011).
- E. O. Chi, W. S. Kim, and N. H. Hur, *Solid State Commun.* **120**(7–8), 307 (2001).
- J. Lin, B. Wang, P. Tong, S. Lin, W. Lu, X. Zhu, Z. Yang, W. Song, J. Dai, and Y. Sun, *Scr. Mater.* **65**, 452 (2011).
- S. Lin, B. Wang, J. Lin, Y. Huang, W. Lu, B. Zhao, P. Tong, W. Song, and Y. Sun, *Appl. Phys. Lett.* **101**, 011908 (2012).
- P. Sun, M. Zhu, K. Wang, M. Zhong, J. Wei, D. Wu, and H. Zhu, *ACS Appl. Mater. Interfaces* **5**, 9563 (2013).
- S. Cho, K. Kikuchi, E. Lee, M. Choi, I. Jo, S.-B. Lee, S.-K. Lee, and A. Kawasaki, *Sci. Rep.* **7**(1), 14943 (2017).
- C. Adelman, *Solid State Electron.* **152**, 72 (2019).
- H. A. Schafft, S. Mayo, S. N. Jones, and J. S. Suehle, in *Proceedings of 1994 IEEE International Integrated Reliability Workshop (IRWS)* (IEEE, 1994), p. 5.
- A. Von Glasow, A. Fischer, and G. Steinlesberger, in *2003 IEEE International Reliability Physics Symposium Proceedings* (IEEE, 2003), p. 126.
- D. Meindl, *Comput. Sci. Eng.* **5**, 20 (2003).
- T. Dinh, H.-P. Phan, A. Qamar, P. Woodfield, N.-T. Nguyen, and D. V. Dao, *J. Microelectromech. Syst.* **26**, 966 (2017).
- H. J. K. Kim, K. E. Kaplan, P. Schindler, S. Xu, M. M. Winterkorn, D. B. Heinz, T. S. English, J. Provine, F. B. Prinz, and T. W. Kenny, *ACS Appl. Mater. Interfaces* **11**, 9594 (2019).
- T. Schössler, F. Schön, C. Lemier, and G. Urban, *Thin Solid Films* **698**, 137877 (2020).
- Q. Zhang, X. Zhang, B. Cao, M. Fujii, K. Takahashi, and T. Ikuta, *Appl. Phys. Lett.* **89**, 114102 (2006).
- K. Gregorczyk, P. Banerjee, and G. W. Rubloff, *Mater. Lett.* **73**, 43 (2012).
- A. Maffucci, F. Micciulla, A. E. Cataldo, G. Miano, and S. Bellucci, *IEEE Trans. Compon. Packag. Manuf. Technol.* **7**, 485 (2017).
- S. Dutta, S. Kundu, A. Gupta, G. Jamieson, J. F. G. Granados, J. Bömmels, C. J. Wilson, Z. Tökei, and C. Adelman, *IEEE Electron. Device Lett.* **38**, 949 (2017).
- G. P. Szakmany, A. O. Orlov, G. H. Bernstein, and W. Porod, *IEEE Trans. Nanotechnol.* **13**(6), 1234 (2014).
- C. L. Petersen, T. M. Hansen, P. Bøggild, A. Boisen, O. Hansen, T. Hassenkam, and F. Grey, *Sens. Actuators A* **96**, 53 (2002).
- D. Worledge and P. Trouilloud, *Appl. Phys. Lett.* **83**, 84 (2003).
- D. H. Petersen, O. Hansen, T. M. Hansen, P. Bøggild, R. Lin, D. Kjær, P. F. Nielsen, T. Clarysse, W. Vandervorst, E. Rosseel, N. S. Bennett, and N. E. B. Cowern, *J. Vac. Sci. Technol. B* **28**(1), 27 (2010).
- F. Smits, *Bell Syst. Tech. J.* **37**, 711 (1958).
- A. Uhlir Jr., *Bell Syst. Tech. J.* **34**, 105 (1955).
- D. Kjær, R. Lin, D. H. Petersen, P. M. Kopalidis, R. Eddy, D. A. Walker, W. F. Egelhoff, and L. Pickert, *AIP Conf. Proc.* **1066**, 167 (2008).
- S. Thorsteinsson, F. Wang, D. H. Petersen, T. M. Hansen, D. Kjær, R. Lin, J.-Y. Kim, P. F. Nielsen, and O. Hansen, *Rev. Sci. Instrum.* **80**, 053902 (2009).
- E. Rosseel, D. H. Petersen, F. W. Osterberg, O. Hansen, J. Bogdanowicz, T. Clarysse, W. Vandervorst, C. Orttoland, T. Hoffmann, and P. Chan, in *2009 17th International Conference on Advanced Thermal Processing of Semiconductors* (IEEE, 2009), p. 1.
- D. M. Mackenzie, K. G. Kalhauge, P. R. Whelan, F. W. Østergaard, I. Pasternak, W. Strupinski, P. Bøggild, P. U. Jepsen, and D. H. Petersen, *Nanotechnology* **31**, 225709 (2020).
- J. Bogdanowicz, S. Folkersma, S. Sergeant, A. Schulze, A. Moussa, D. H. Petersen, O. Hansen, H. H. Henrichsen, P. F. Nielsen, and W. Vandervorst, *Phys. Status Solidi A* **215**, 1700857 (2018).
- S. Folkersma, J. Bogdanowicz, A. Schulze, P. Favia, D. H. Petersen, O. Hansen, H. H. Henrichsen, P. F. Nielsen, L. Shiv, and W. Vandervorst, *Beilstein J. Nanotechnol.* **9**, 1863 (2018).
- K. Serbulova and Y. Vountesmy, in *2019 IEEE 39th International Conference on Electronics and Nanotechnology (ELNANO)* (IEEE, 2019), p. 369.
- D. C. Gupta and J. Y. Chan, *Rev. Sci. Instrum.* **41**(2), 176 (1970).
- S. O. Kasap, *Principles of Electronic Materials and Devices* (Tata McGraw-Hill, 2006).

- <sup>43</sup>D. W. Koon, F. Wang, D. H. Petersen, and O. Hansen, *J. Appl. Phys.* **114**(16), 163710 (2013).
- <sup>44</sup>S. Director and R. Rohrer, *IEEE Trans. Circuit Theory* **16**(3), 318 (1969).
- <sup>45</sup>J. L. Riddle, G. T. Furukawa, and H. H. Plumb, *Platinum Resistance Thermometry* (National Bureau of Standards, 1973).
- <sup>46</sup>H. S. Carslaw and J. C. Jaeger, *Conduction of Heat in Solids* (Clarendon Press, 1959).
- <sup>47</sup>H.H. Henrichsen, O. Hansen, D. Kjær, P.F. Nielsen, F. Wang, and D. H. Petersen, in *2014 International Workshop on Junction Technology* (IEEE, 2014), p. 1.
- <sup>48</sup>L. J. van der Pauw, *Philips Tech. Rev.* **20**, 220 (1958).
- <sup>49</sup>T. Ansbæk, D. H. Petersen, O. Hansen, J. B. Larsen, T. M. Hansen, and P. Bøggild, *Microelectron. Eng.* **86**, 987 (2009).
- <sup>50</sup>M. Yerry and M. Shephard, *IEEE Comput. Graph. Appl.* **1**, 39 (1983).
- <sup>51</sup>P. O. Persson and G. Strang, *SIAM Rev.* **46**(2), 329 (2004).
- <sup>52</sup>COMSOL Multiphysics® v.5.5, COMSOL AB, Stockholm, Sweden, see [www.comsol.com](http://www.comsol.com).
- <sup>53</sup>M. Kockert, R. Mitdank, A. Zykov, S. Kowarik, and S. F. Fischer, *J. Appl. Phys.* **126**(10), 105106 (2019).
- <sup>54</sup>I. K. Harvey and H. Collins, *Rev. Sci. Instrum.* **44**, 1700 (1973).
- <sup>55</sup>J. Bojkovski, V. Zuzek, V. Batagelj, and J. Drnovsek, in *11th International Conference on Heat Transfer, Fluid Mechanics and Thermodynamics* (International Conference on Heat Transfer, Fluid Mechanics and Thermodynamics, 2015).
- <sup>56</sup>G. Fernqvist, P. Dreesen, G. Hudson, and J. Pickering, in *2007 IEEE Particle Accelerator Conference (PAC)* (IEEE, 2007), p. 317.
- <sup>57</sup>T. E. Dinan, U.S. Patent 6,037,790 (International Business Machines Corp., 2000).